Hubble Deep Field Constraint on Baryonic Dark Matter

Chris Flynn

Tuorla Observatory, Piikkiö, FIN-21500, Finland

Andrew Gould[⋆]

Dept of Astronomy, Ohio State University, Columbus, OH 43210

John N. Bahcall

Institute For Advanced Study, Princeton, NJ 08540

cflynn@astro.utu.fi, gould@payne.mps.ohio-state.edu, jnb@ias.edu

Abstract

We use a new technique to search for faint red stars in the Hubble Deep Field. We distinguish unambiguously between stars and galaxies to I = 26.3. Our results place strong and general constraints on the I-band luminosity of the constituents of the Galactic dark halo.

Subject Headings: dark matter – gravitational lensing – stars: low mass, brown dwarfs, luminosity function

⋆ Alfred P. Sloan Foundation Fellow

1. Introduction

The detection of ~ 7 candidate microlensing events by the MACHO collaboration (Alcock et al. 1993, 1995, 1996a,b) during two years of observations toward the Large Magellanic Cloud (LMC) implies that a significant fraction ($0.2 \lesssim f \lesssim 1$) of the dark halo of the Galaxy may be in the form of massive compact halo objects (MACHOs). The mean observed time scale of the events is $\langle t_e \rangle \sim 37\,$days, where t_e is the Einstein radius crossing time. This time scale is substantially longer than would be expected if the MACHOs have sub-stellar masses, $M \lesssim 0.1\,M_\odot$, and if their velocity and spatial distributions were in accord with a standard halo model. Within the context of such a model, the best estimate for the mean mass is $\langle M \rangle \sim 0.4\,M_\odot$, with a range $0.1 \lesssim \langle M \rangle / M_\odot \sim 1$ at the $3\,\sigma$ level. The EROS collaboration (Aubourg et al. 1993, 1995; Ansari et al. 1996), has detected two candidate events from a somewhat smaller data set and with a somewhat shorter mean time scale $\langle t_e \rangle = 26\,$days. The EROS data are consistent with the results inferred from the MACHO data. These long duration events contribute heavily to both the high estimate of the total MACHO density and the high inferred mean mass of the detected objects.

If there is a substantial population of MACHOs, then it is possible that some of these objects may be luminous enough and close enough to be directly detected in optical light. Red dwarfs were a plausible candidate of this type. Bahcall et al. (1994, hereafter Paper I) searched for such objects in deep images taken by the Wide Field Camera (WFC2) on the *Hubble Space Telescope (HST)* to a limiting magnitude of $I = 25.3$. From the null results of that search, they concluded that faint red dwarfs ($M_I < 14$) make up $< 6\%$ of the Galactic halo. With additional plausible assumptions, Graff & Freese (1996) have derived even stronger constraints using the same observational results.

The new results of MACHO (Alcock et al. 1996b) may point in a different direction: white dwarfs (WDs). Although several arguments appear to constrain the WD contribution to the halo to be $< 10\%$ (Charlot & Silk 1995) or $< 25\%$

(Adams & Laughlin 1996), the fact that MACHO may be detecting objects in the WD mass range means that this candidate must be taken seriously. More generally, the nature of the detected objects, whatever they are, can be probed or constrained by searching for intrinsically faint stars.

The Hubble Deep Field (HDF) (Williams et al. 1996) taken with WFC2 on *HST* provides a unique window on the universe (Bahcall, Guhathakurta, & Schneider 1990; Abraham et al. 1996; Colley & Rhoads 1996). The extreme depth of the HDF, which has an equivalent exposure time ~ 10 greater than the field analyzed in Paper I, provides an unprecedented opportunity to find faint stellar objects. The principal advantage of going deep is that it allows one to search for faint stars in regions of the color-magnitude diagram (CMD) which are virtually devoid of the stars that populate the standard Galactic components. The lack of ordinary disk and spheroid stars at very faint magnitudes is a result of the finiteness of the Galaxy. Thus, by restricting attention to objects within 1.67 mag of the magnitude limit, one probes 90% of the available volume for intrinsically faint stars while eliminating nearly all of the stars from previously well-studied Galactic populations. Of course, by going deep one also increases the total volume probed (for candidate objects of fixed luminosity) but this advantage is secondary: a survey of 16 fields each 2 mag less deep would have the same volume and would require only 40% of the telescope time. However, these fields would contain of order 30 dwarf and sub-dwarf Galactic stars within 1.67 mag of the magnitude limit, where we have made the estimate based on actual star counts in the *HST* Large Area Multi-Color Survey ("Groth Strip", $l = 96°$, $b = 60°$). Hence, the HDF provides a truly unique opportunity to search for intrinsically faint stars.

In § 2, we describe our technique for discriminating stars from extended objects to a magnitude limit of $I = 26.3$. In § 3, we discuss our selection criteria and report that no stars are detected. In § 4, we show that the lack of detections means that if the Galactic halo is composed of WDs of mass $M = 0.5\,M_\odot$, these must have $M_I > 15.9$ (or $M_V \gtrsim 18.4$). For red dwarfs and brown dwarfs of mass $0.08\,M_\odot$, the limit is stronger, $M_I > 17.2$.

2. Finding Stars in the HDF

Objects can be detected in HDF down to $I \sim 28$, the great majority of which are galaxies. For star counts it is essential to distinguish unambiguously between the handful of stars and the thousands of background galaxies. Distinguishing stellar from extended profiles requires ~ 5 times more photons than just detection, so the magnitude limit for star counts is much brighter than the detection limit, as quantified below.

We introduced in paper I a procedure for separating stars and galaxies based on the radial profiles of the objects. The empirical stellar radial profile on WFC2 was determined from a large number of stars on a WFC2 exposure at low galactic latitude. Many stars (falling at random places relative to the pixel grid) were required because the WFC2 poorly samples the point spread function (PSF). (The PSF full width half maximum is approximately 1.2 pixels. See Fig. 1, below.)

The HDF exposures were taken in groups at a number of positions on the sky (these groupings are termed "dithers"), each offset slightly relative to the HDF field center, in order to improve the spatial resolution and the smoothness of the flatfielding corrections. The HDF team released special "drizzled" images in four filters, (F300, F450, F606, and F814) produced using a "drizzling" technique (Fruchter & Hook 1996), which takes into account the shifts and rotations between the individual dither positions and geometric distortions at the image plane, while preserving the flux.

Drizzling involves the rebinning of undersampled data, and the radial profiles of sources in the drizzled image are slightly different from those in the original images. Hence, to find the stars in HDF we developed a procedure that combines the depth of the drizzled image with the well-understood PSF properties of the raw data.

We obtained flatfielded and bias-subtracted frames from the Space Telescope Science Institute. Some of the frames were affected by significant scattered light from Earth. The HDF team ignored these frames in constructing their first-release drizzled images, and we followed their example in this respect. (By exposure time, 6% of the F606 and 25% of the F814 frames were not used). HST's high pointing and tracking accuracy means that the frames at each dither position are precisely aligned, so stacking and cleaning (i.e. removing hot pixels and cosmic rays) the images in each dither is straightforward, and we used the procedure as in Paper I to create cleaned images at each dither position. The total exposure time in F814 was 92,200 s in 39 separate exposures, taken at 8 separate dither positions, and in F606 was 110,050 s in 105 exposures at 11 dither positions.

We searched the drizzled F814 band image for sources down to a magnitude limit of $I = 26.5$, beyond which the radial profiles on the dithered frames become too noisy to classify reliably. We required that the ratio of peak to total flux be at least half as large as the value found for known stars. This initial selection yielded 629 objects. Each object was then located on the 19 dither frames (8 in F814 and 11 in F606). The radial profile of the object on each of the dither images was determined independently, and these were plotted against the empirical stellar profile for the filters F814 and F606 (as determined in Paper I).

The key to star/galaxy separation is that we can locate the center of a stellar image to an accuracy of better than 0.1 pixels, using the symmetry of the stellar image about its center. Thus, for any given star on any given dither, we can construct a radial profile of the image which gives the fraction of light in each pixel as a function of the distance of the pixel from the center of the stellar light. Because the centers of the stars fall on the various dither images over a good range of spatial positions relative to the pixel grid, superimposing the radial profiles from the separate dithers gives us a densely sampled profile,

Figure 1(a) shows an object of moderate signal to noise, which we classify as a star (this object appears on Chip 4 of the drizzled images at $(x, y) = (350, 598)$ and has $I = 23.71$, $V - I = 1.32$). The densely sampled radial profile from the 8 independently centered dither images (shown as circles) matches the empirical stellar profile (shown as a line) very well. Figure 1(b) shows the profile of this star from a single dither. Note that for only three pixels does the pixel center fall within one pixel of the center of the star. However, these three points are sufficient to distinguish stars from galaxies provided that the galaxies are extended by $\gtrsim 1$ pixels, i.e. $\gtrsim 0\farcs1$. We used plots of this type in Paper I and in Gould, Bahcall, & Flynn (1996) to identify stars in 22 WFC2 fields. In Figure 1(c), we show the profile of the same object as seen in the drizzled image, where we take into account the different pixel size (drizzled pixels are a factor of 0.402 smaller). The drizzled profile begins to deviate from the WFC2 profile at about 0.6 pixels.

We compared the densely sampled profile with the drizzled profile for several dozen stellar and nearly stellar objects. We found that for objects $I \lesssim 25.5$, stars could be easily distinguished from galaxies using either profile. However, for $I \gtrsim 25.5$ we found several objects whose densely sampled profiles are clearly non-stellar, but which could not be distinguished from stars using the drizzled profile. Because of the difficulties in classifying objects on the drizzled image, we identify candidate objects on the drizzled image but do the classification on the 19 dither images.

Diagrams similar to Figure 1(a) were made for each of the 629 objects found on the drizzled F814 frame, and CF and AG independently classified them as either "star", "galaxy", "quasi-stellar", or "?". The designation "quasi-stellar" means that the object is clearly not a star, but deviates from a stellar profile only within 1 pixel. Objects were then photometered using the same aperture size and calibration from F814 and F606 to I, $V-I$ as in Paper I. Comparison of the classifications by CF and AG showed that we could classify stars and galaxies with confidence to $I = 26.2$. We found a total of 17 stellar objects to this limit. In addition, we found 1 blue stellar object beyond the magnitude limit ($I = 26.5$, $V - I = 0$). All stellar objects satisfying the I band magnitude limit were easily detected and photometered in V. Photometric errors were estimated from the scatter of the measurements made from different dithers and are ~ 0.08 mag at the magnitude limit and ~ 0.03 mag at $I = 25$. The uncertainties induced by photometric errors are therefore several orders of magnitude smaller than the Poisson uncertainties.

3. Selection Criteria

Figure 2 is a CMD of the stars detected in the HDF together with the adopted selection criteria, which are described below. First, we restrict attention to red stars, $V - I > 1.8$, which includes M dwarfs, and is expected to include brown dwarfs and old WDs. The local density of old *disk* WDs has been measured by proper-motion studies to $M_V = 17$ (corresponding to $V - I \sim 1.8$) (Liebert, Dahn, & Monet 1988). Halo WDs, which are expected to be fainter than this limit, would not have shown up in this study because their proper motions μ would generally exceed the selection limit of $\mu < 2.''5\,\mathrm{yr}^{-1}$ (or perhaps somewhat smaller).

Second, we set the magnitude limit at $I_{\rm max} = 26.30$. As discussed in the previous section, we find that our star/galaxy separation is reliable for $I < 26.2$. The brightest object above this limit that lies in the adopted color range and is not obviously a galaxy has $I = 23.39$. We therefore have detected all stars to $I = 26.3$.

Third, we establish a lower magnitude limit $I_{\rm min}$ so as to exclude ordinary Galactic stars. As discussed in the introduction, the HDF is so deep that one expects very few ordinary stars near the magnitude limit. By setting $I_{\rm min} = I_{\rm max} - 1.67 = 24.63$, we therefore exclude the regions of the CMD that are heavily populated with previously well-studied stars, while preserving 90% of the total volume. Figure 2 shows that, with the above-described criteria, the color-magnitude diagram is devoid of stars in the region, $24.63 < I < 26.30$, $V - I > 1.8$

Finally, we note that for $V - I \lesssim 0.7$, there are ~ 60 compact non-stellar objects that lie near the magnitude limit. Since some of these objects deviate from point sources only in the inner fraction of a pixel ($< 0.''1$), one must wonder whether there are not other objects of this class which appear perfectly stellar. Indeed, we find three such faint stellar objects with A-star colors and $I \sim 26$ (see Fig. 2), and are currently investigating the nature of these extremely compact objects as a whole. The presence of this class of object complicates the search for faint blue stars. However, since they are well blueward of the "halo zone", they have no impact on the principal results of the present paper.

4. Limits

Since we detect no objects with $V - I > 1.8$, we can rule out at the 95% confidence level any model that predicts 3.0 or more detections in this regime. In particular, since the HDF goes 1 magnitude deeper than the field used in Paper I, we can immediately extend the results derived there. For red dwarfs brighter than $M_I = 15$ (the faintest red dwarf ever seen, Monet et al. 1992) the halo fraction must be $f < 6\%$. For $M_I < 14$, the fraction is $\lesssim 1\%$.

To further interpret these results, consider a class of objects each with mass M that comprise a fraction f of the dark halo, and so have a local number density $n = f\rho_0/M$ where $\rho_0 = 9\times10^{-3}\,M_\odot\,\mathrm{pc}^{-3}$ is taken as the local halo density (Bahcall, Schmidt, & Soneira 1983). Now suppose that these objects are detectable out to a distance d within the HDF with angular area $\Omega = 4.4\,\mathrm{arcmin}^2$. Then the number of expected detections N_{exp} is

$$N_{\mathrm{exp}} = \frac{1}{3}n\Omega d^3 = 3f\left(\frac{M}{0.5\,M_\odot}\right)^{-1}\left(\frac{d}{1.1\,\mathrm{kpc}}\right)^3, \qquad (4.1)$$

where we have assumed initially that the halo density is uniform over the region probed. In fact, equation (4.1) shows that one can begin to place limits on objects that can be detected to $d \sim$ 1–2 kpc, where the exact distance limit d depends only weakly on the details of the model. For simplicity, we adopt a halo with density $\propto r^{-2}$ which has a local density $\rho_h = 0.86\rho_0$ at a distance of 1.5 kpc in the direction of the HDF ($l = 126^\circ, b = 55^\circ$). Since the magnitude limit is $I < I_{\mathrm{max}} = 26.30$ and since 10% of the volume is excluded by selecting $I > I_{\mathrm{min}} = 24.63$, we find a limit

$$M_I > 15.9 + \frac{5}{3}\log\left(f\frac{0.5M_\odot}{M}\right) \qquad (V - I > 1.8). \qquad (4.2)$$

That is, for objects brighter than this limit there are more than 3 expected detections, contrary to the observations.

For WDs of mass $M = 0.5\,M_\odot$ and $V - I > 1.8$, these limits imply $M_I > 15.9 + 1.67\log(f)$. To interpret this limit as a limit on the halo fraction, we assume that the observed linear color-magnitude relation for the red end of the disk WDs (Monet et al. 1992), $M_I = 12.9 + 1.2(V - I)$, can be extended to the fainter halo WDs. We then find limits on the halo fraction f of

$$f < 0.31 \times 10^{0.72[(V-I)-1.8]}. \tag{4.3}$$

Hence, under these assumptions, a full WD standard halo is ruled out for $V - I < 2.5$ ($M_V < 18.4$) and a 33% WD standard halo is ruled out for $V - I = 1.8$ ($M_V = 16.9$), both at the 95% confidence level.

We now compare the sensitivity of our results with the measurements of and constraints on luminous halo objects obtained with a variety of techniques as reviewed by Mould (1996). Generally, if one is interested in objects that are at least as bright as the end of the locally observed sub-dwarf sequence ($M_V \sim 15$, $V - I \sim 3$), then there are several probes that are at least as sensitive than the one presented here. For example, Dahn et al. (1995) use proper-motion selected stars to construct a luminosity function. Based on this model, we expect to find $\lesssim 1$ star with $V - I > 1.8$. Similarly, the deep color-selected ground-based survey of Boeshaar et al. (1994) can detect such objects over ~ 3 times the volume probed by HDF (although such surveys are subject to significant contamination by faint galaxies). The real strength of the HDF is its sensitivity to intrinsically faint objects, near the limit (4.2). These would have avoided detection in proper-motion surveys. For red objects ($V - I \gtrsim 3.5$), the volume probed by HDF is larger than for any ground-based photometric surveys and, of course, HDF is free of galaxy contamination.

Finally, we note that the HDF star counts can be used to constrain the density of Local Group stars. Local Group giants and sub-giants $M_I \lesssim 1.5$, $0.6 \lesssim V - I \lesssim 1.5$ could be seen to a distance $d \sim 0.9\,\mathrm{Mpc}$. In the outer 90% of this volume, there are no more than 2 such stars observed, implying that their density must be

$< 7 \times 10^{-11}\,\mathrm{pc}^{-3}$ at the 95% confidence level. Comparing this limit to the density of local spheroid giants $\sim 2 \times 10^{-7}\,\mathrm{pc}^{-3}$ (Morrison, 1993; Flynn & Fuchs 1994) we constrain the ratio of the densities of Local Group to galactic spheroid stars to be $< 1/3000$, about an order of magnitude lower than the limits obtained by Richstone et al. (1992).

Acknowledgements: We are grateful to K. Griest and P. Sackett for valuable comments. We thank the Director of STScI, Robert Williams, and the HDF-team for skillful execution of the HDF concept and for rapidly reducing and making available the superb images. A. G. was supported in part by NSF grant AST 9420746. J. N. B. was supported in part by NASA grant NAG5-1618. The work is based in large part on observations with the NASA/ESA Hubble Space Telescope, obtained at the Space Telescope Science Institute, which is operated by the Association of Universities for Research in Astronomy, Inc. (AURA), under NASA contract NAS5-26555.

REFERENCES

1. Abraham, R. G., Tanvir, N. R., Santiago, B. X., Ellis, R. S., & Glazebrook, K. 1996, MNRAS, in press
2. Adams, F. C. & Laughlin, G. 1996, ApJ, submitted
3. Alcock, C., et al. 1993, Nature, 365, 621
4. Alcock, C., et al. 1995, Phys. Rev. Lett. 74, 2867
5. Alcock, C., et al. 1996a, 461, 84
6. Alcock, C., et al. 1996b, in preparation
7. Aubourg, E., et al. 1993, Nature, 365, 623
8. Aubourg, E., et al. 1995, A&A, 301, 1
9. Ansari, R. et al. 1996, A&A, in press
10. Bahcall, J.N., Flynn, C., Gould, A., & Kirhakos, S. 1994, ApJ, 435, L51 (Paper I)
11. Bahcall, J. N., Guhathakurta, P. & Schneider, D. P. 1990, Science, 248, 178
12. Bahcall, J. N., Schmidt, M., & Soneira, R. M. 1983, ApJ, 265, 730
13. Boeshaar, P. C., Tyson, T., & Bernstein, G. 1994, BAAS, 185, 1346
14. Charlot, S. & Silk, J. 1995, ApJ, 445, 124
15. Colley, W. N. & Rhoads, J. E. 1996, preprint
16. Dahn, C. C., Liebert, J. W., Harris, H., & Guetter, H. C. 1995, p. 239, An ESO Workshop on: the Bottom of the Main Sequence and Beyond, C. G. Tinney ed. (Heidelberg: Springer)
17. Flynn, C. & Fuchs, B. 1994, MNRAS, 270, 471
18. Fruchter, A. S. & Hook, R. 1996 http://www.stsci.edu/ftp/observer/hdf/combination/drizzle.ht
19. Gould, A., Bahcall, J. N., & Flynn, C. 1996, ApJ, 465, 000

20. Graff, D., & Freese, K. 1996, ApJ, 456, L49

21. Liebert, J., Dahn, C. C., & Monet, D. G. 1988, ApJ, 332, 891

22. Monet, D. G., Dahn, C. C., Vrba, F. J., Harris, H. C., Pier, J. R., Luginbuhl, C. B., & Ables, H. D. 1992, AJ, 103, 638

23. Morrison, H. 1993, AJ, 106, 587

24. Mould, J. 1996, PASP, 108, 35

25. Richstone, D. O., Gould, A., Guhathakurta, P., & Flynn, C. 1992, ApJ, 388, 354

26. Williams, R. et al. 1996, Science with the Hubble Space Telescope II, P. Benvenuti, F. D. Macchetto, & E. J. Schreier, eds., in press (Baltimore: STScI)

FIGURE CAPTIONS

1) (a) A densely sampled light profile of a test object (*circles*) is compared to the template profile of a star (*solid line*) that is constructed from a WFC2 image of stars in a low-latitude field (see Paper I). Each circle represents one pixel in one of the 8 WFC2 dither images of HDF taken with the F814 filter. The distance (in pixels) from the center of the star to the center of the pixel is plotted against the fraction of all star light from the dither image falling on that pixel. Note that even though the individual dither images are highly undersampled, the combined profile is well sampled to well within 1 pixel. The close agreement with the template indicates that the object is stellar. (b) Same as (a) except that only one of the eight dither images is shown. (c) Profile constructed from the single drizzled image. Vertical and horizontal axes have been adjusted to account for the difference in pixel size. Note that the profile is nearly identical to the template profile except within 0.6 pixels of the center.

2) Color-magnitude diagram ($V - I$ vs I) of stellar objects detected in HDF. The errors are not shown since they would be of order or smaller than the size of the points. The selection criteria delimiting the "halo zone" are shown as a box at the lower right. These are $I < 26.30$ (magnitude limit for star/galaxy discrimination), $I > 24.83$ (eliminate ordinary Galactic stars while keeping 90% of the volume probed), and $V - I > 1.8$ (color region of interest for dark halo candidates).

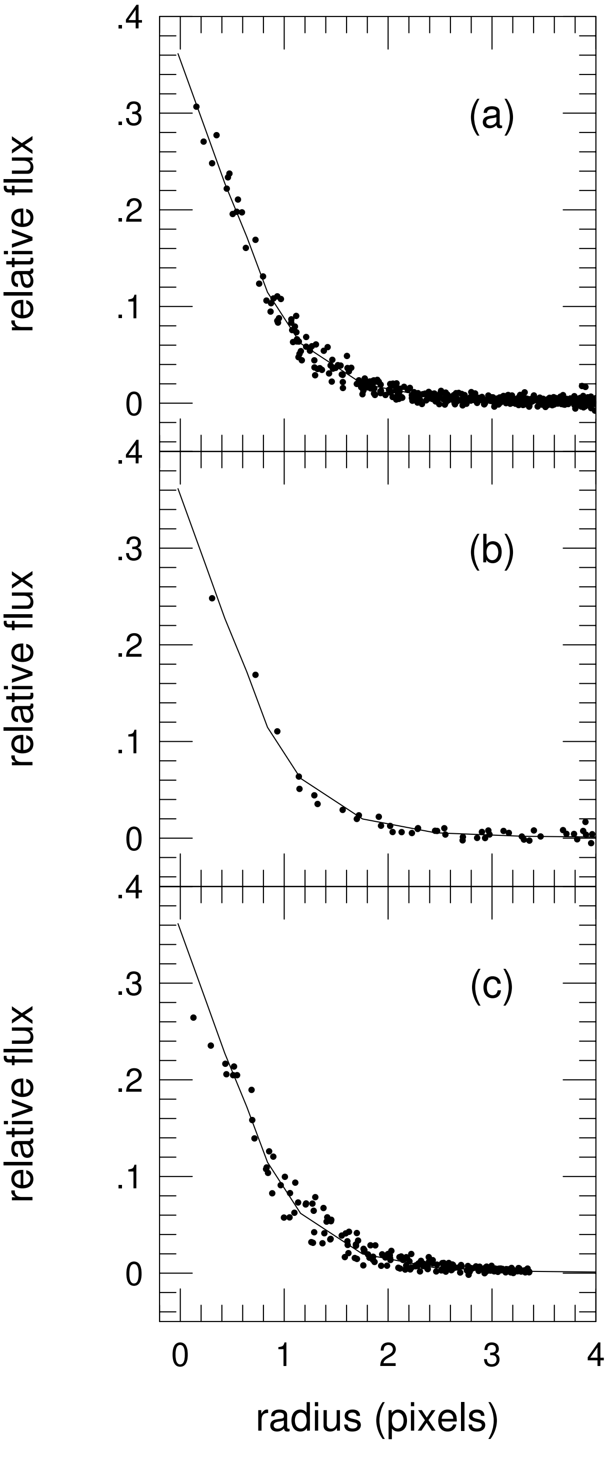
(a)
(b)
(c)
relative flux
relative flux
relative flux
.4
.3
.2
.1
0
.4
.3
.2
.1
0
.4
.3
.2
.1
0
0
1
2
3
4
radius (pixels)

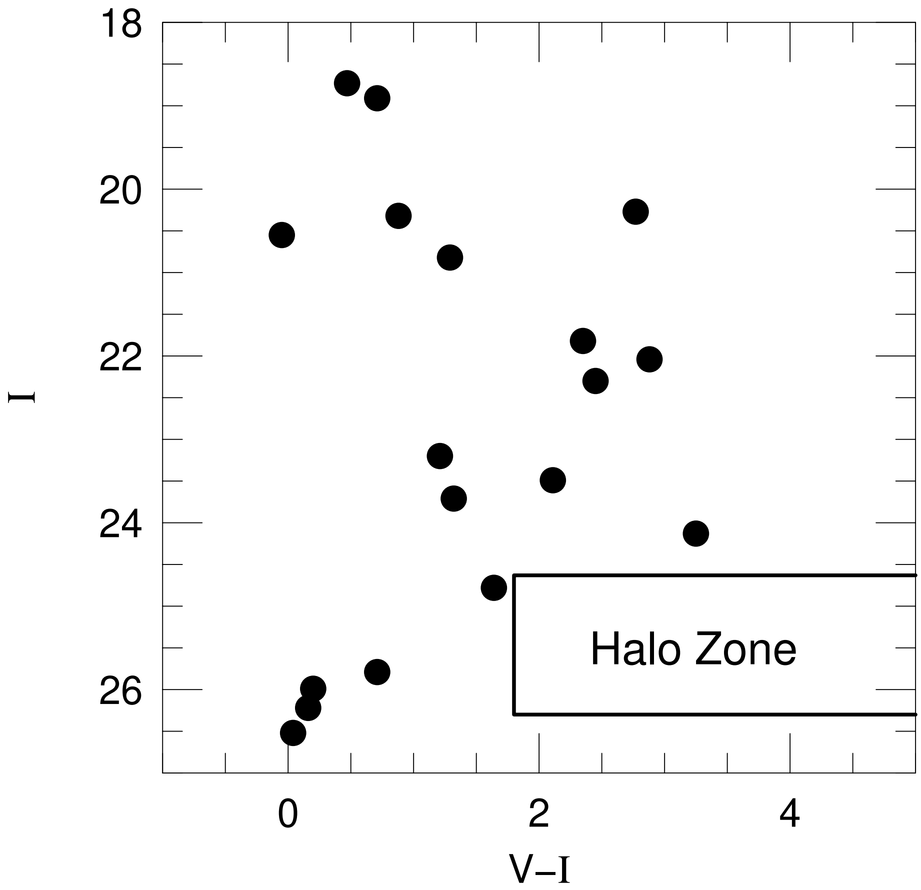

18
20
22
24
26
I
0
2
4
V−I
Halo Zone